Butane dihedral angle dynamics in water is dominated by internal friction

Jan O. Daldrop[1], **Julian Kappler**[1], **Florian N. Brünig**[1], and **Roland R. Netz**[1,2]

[1] Freie Universität Berlin, Department of Physics, 14195 Berlin, Germany

This manuscript was compiled on January 25, 2018

The dihedral dynamics of butane in water is known to be rather insensitive to the water viscosity, possible explanations for this involve inertial effects or Kramers' turnover, the finite memory time of friction, and the presence of so-called internal friction. In order to disentangle these factors, we introduce a method to directly extract the friction memory function from simulations in the presence of an arbitrary free-energy landscape. By analysis of the dihedral friction in butane for varying water viscosity, we demonstrate the existence of an internal friction contribution. At normal water viscosity the internal friction turns out to be eight times larger than the solvent friction and thus completely dominates the effective friction. By comparison with simulations of a constrained butane molecule that has the dihedral as the only degree of freedom, we show that internal friction comes from the six additional degrees of freedom in unconstrained butane that are orthogonal to the dihedral angle reaction coordinate. While the insensitivity of butane's dihedral dynamics to water viscosity is solely due to the presence of internal friction, inertial effects nevertheless crucially influence the resultant transition rates. In contrast, non-Markovian effects due to the finite memory time are present but do not significantly influence the dihedral barrier crossing rate of butane. These results not only settle the character of dihedral dynamics in small molecular systems such as butane, they also have important implications for the folding of polymers and proteins.

molecular friction | reaction rates | memory effects

For the understanding of conformational and biochemical reactions, a low-dimensional stochastic description in suitable reaction coordinates is a powerful approach. In particular in the context of protein folding, diffusion in a one-dimensional free-energy landscape is a prominent model to come to terms with the high-dimensional phase-space dynamics of proteins (1–3). By projection onto a one-dimensional reaction coordinate, orthogonal degrees of freedom produce effective friction and random force contributions (4, 5). These byproducts of projection cannot be neglected, since friction decisively influences reaction rates (6).

Obviously, the friction that characterizes a protein folding coordinate contains contributions from the surrounding solvent as well as from internal protein degrees of freedom (7), but it is less clear how to separately measure these two contributions (experimentally or in simulations). Typically, the prime object in protein studies concerned with friction effects is the folding time τ_{fold}. In the overdamped limit, when inertia and memory effects are neglected, τ_{fold} scales with the effective friction coefficient γ as $\tau_{\text{fold}} \sim \gamma^{-1}$ (6). By the addition of viscogenic agents the solvent viscosity η increases relative to the pure water value; assuming that solvent and internal friction are additive according to $\gamma = \gamma_{\text{sol}} + \gamma_{\text{int}}$ and furthermore that Stokes' law holds for the solvent friction contribution, $\gamma_{\text{sol}} \sim \eta$, the internal contribution γ_{int} can be obtained by linear

extrapolation of $\tau_{\text{fold}}^{-1} \sim \gamma_{\text{sol}} + \gamma_{\text{int}}$ down to vanishing solvent viscosity (7). Via this procedure, internal friction has been demonstrated for various proteins (7–16). In fact, deviations from a linear dependence $\gamma_{\text{sol}} \sim \eta$ have been experimentally observed for some proteins (9), while for other proteins no internal friction was detected at all (17). Even in simulations, where—in contrast to experiments—the water friction can be reduced and a modification of the folding free energy landscape with changing viscosity can be excluded, the extrapolation down to vanishing solvent friction is not trivial (18–22).

The above definition of internal friction hinges on a few critical assumptions which are not necessarily satisfied in real systems: i) It was pointed out that inertia effects lead to deviations from the simple law $\tau_{\text{fold}} \sim \gamma^{-1}$ and ultimately to Kramers turnover, which can be misinterpreted as internal friction (23–25). While one would intuitively think that the effective mass of a protein reaction coordinate is small, the balance of effective inertial and friction parameters of reaction coordinates that describe complex reactions is not really settled. ii) Friction will in general not be constant along a reaction coordinate (15, 18), so the linear additivity assumption $\gamma = \gamma_{\text{sol}} + \gamma_{\text{int}}$ not necessarily holds when averaged over the reaction coordinate and needs to be checked directly. iii) Most serious are memory effects, which decisively influence barrier crossing dynamics (19). Recently it was shown that memory effects can, depending on the value of the memory time, slow down or even accelerate barrier crossing (26), which starkly invalidates the overdamped Kramers scaling $\tau_{\text{fold}} \sim \gamma^{-1}$.

Previous theoretical approaches to internal friction are based on reaction times, they suffer from the indirect connection between transition times and friction and necessarily rely on various model assumptions (18–22) (not so different from

---

Significance Statement

The interpretation of rates of reactions that take place in a solvent is complicated because of the entanglement of free-energy and history-dependent friction effects. In this context, the dihedral dynamics of butane has played a paradigmatic role since it is simple yet relevant for conformational transitions in polymers and proteins. Using a novel method we directly extract the friction that governs the dihedral dynamics in butane from simulations. We show that about 89% of the total friction comes from intrinsic butane degrees of freedom that are orthogonal to the dihedral reaction coordinate and only 11% from the solvent friction. This shows that the hydrodynamic estimate of friction severely fails even in the simplest molecular reaction.

---

www.pnas.org/cgi/doi/10.1073/pnas.XXXXXXXXXX

PNAS | January 25, 2018 | vol. XXX | no. XX | 1–6

the experimental situation). Direly needed are models which allow to check for the presence of internal friction independently of any theoretical assumptions that relate friction to reaction times, as well as methods to extract friction and memory functions directly from simulations instead of inferring friction effects indirectly from measured reaction times.

In this paper we introduce methods to meet both challenges. We consider butane, since it is the simplest molecule that shows a non-trivial conformational transition in a solvent and since it has been a testing ground for theoretical and experimental developments (27–31). In fact, dihedral isomerization rates are known to be quite insensitive to the solvent viscosity (19–22, 24, 32–35) which was argued to be due to inertial and memory effects (19, 36, 37). In our work, we first simulate a single butane molecule in water and compare two scenarios, the free scenario, where all four carbons can freely move, subject to bond length and bond angle constraints, and the constrained scenario, where three carbons are fixed in space and only one terminal carbon can move. While the free energy landscape for the dihedral is the same in both scenarios, the transition times differ for high water viscosities (which we modify in our simulations by changing the water mass) by a factor of ten. This unequivocally demonstrates that the additional butane degrees of freedom (which are orthogonal to the dihedral angle) in the free scenario significantly change the effective friction along the reaction coordinate. Secondly, we introduce a method to extract the friction memory kernel that couples to the reaction coordinate, in our case the dihedral angle, from simulation trajectories. A memory kernel accounts for the fact that friction on the molecular scale is not instantaneous but rather depends on the system's history in a non-Markovian manner. Our calculated memory kernels reveal that indeed the friction substantially differs between the constrained and free butane scenarios. The friction coefficients, which follow by an integral over the memory kernels, are used to predict the transition times of the free and constrained butane scenarios in quantitative agreement with direct simulation results, for this we need to use reaction rate theory that accounts for inertial effects. This shows that our theoretical framework, which simultaneously yields reaction times as well as friction effects, is consistent. Finally, the internal friction contribution is extracted from a fit of the extracted total friction versus the water viscosity: for the constrained butane the internal contribution is negligible, as expected, while for the free butane the internal contribution overwhelms the solvent contribution by a factor of eight, which explains why the butane dihedral reaction is rather insusceptible to an increase of the water viscosity.

We unambiguously show that the dihedral angle dynamics of a butane molecule is dominated by internal friction, which stems from the coupled dynamics of the four carbons. This demonstrates that internal friction exists already for the simplest molecular system that possesses a conformational transition, in line with previous works where dihedral angle isomerization has been argued to be a source of internal friction in protein folding (9, 20–22, 34, 35).

1. Results and Discussion

A. Butane dihedral barrier crossing times. In our simulations we place a single butane in a water box and systematically vary the mass of water molecules m_{w} while keeping the butane
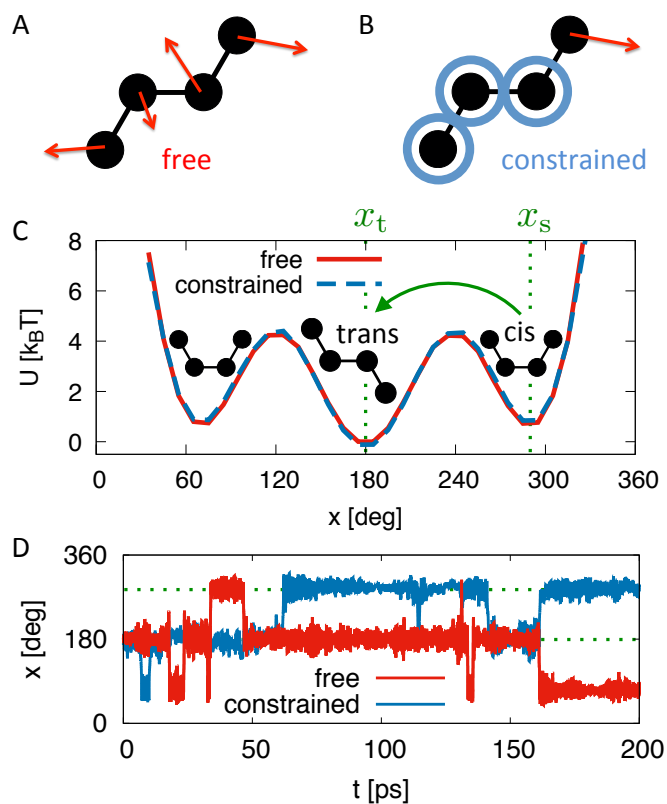
Fig. 1. Schematic illustration of (A) a free butane molecule where all four carbons can move and (B) a constrained butane where three carbons are fixed in space and only one terminal carbon can move. (C) Comparison of the free energy U as a function of the dihedral angle x for the free and constrained butane solvated in SPC/E water, extracted from simulation trajectories. The starting and target angles x_{s} and x_{t} for the calculation of the *cis*-to-*trans* dihedral barrier crossing time are indicated by dotted vertical lines. (D) Typical dihedral angle simulation trajectories for free and constrained butane for elevated water viscosity $\eta = \sqrt{10}\eta_0$.

mass fixed. This modifies all intrinsic water time scales and in particular also the water viscosity according to $\eta \propto \sqrt{m_{\mathrm{w}}}$, but leaves all equilibrium distribution functions invariant (18). We use a united-atom force field for butane that neglects the hydrogens and approximates butane by four Lennard-Jones beads that are subject to fixed bond lengths and fixed bond angles, for water we use the SPC/E model (see Materials and Methods). We compare the free scenario, where all four butane carbons can move, with the constrained scenario, where three carbons are fixed in space and only one terminal carbon can rotate, see Fig. 1A and B for an illustration. The only degree of freedom in the constrained scenario is the dihedral angle, while in the free scenario one has six additional degrees of freedom, three translational and three orientational. The free energy profiles in the free and constrained scenarios in Fig. 1C perfectly overlap, as expected based on translational and orientational invariance of the problem.

The mean first-passage times τ_{MFP} for the *cis*-to-*trans* transition of the dihedral, as defined in Fig. 1C and extracted from the simulation trajectories as shown in Fig. 1D, are depicted as a function of the rescaled water viscosity η/η_0 in Fig. 2 for the free and constrained scenarios. Here η_0 denotes the bulk viscosity of water with the normal mass. τ_{MFP} for free butane is rather insensitive to η, in agreement with previous results (19). Constrained butane behaves differently for $\eta > \eta_0$
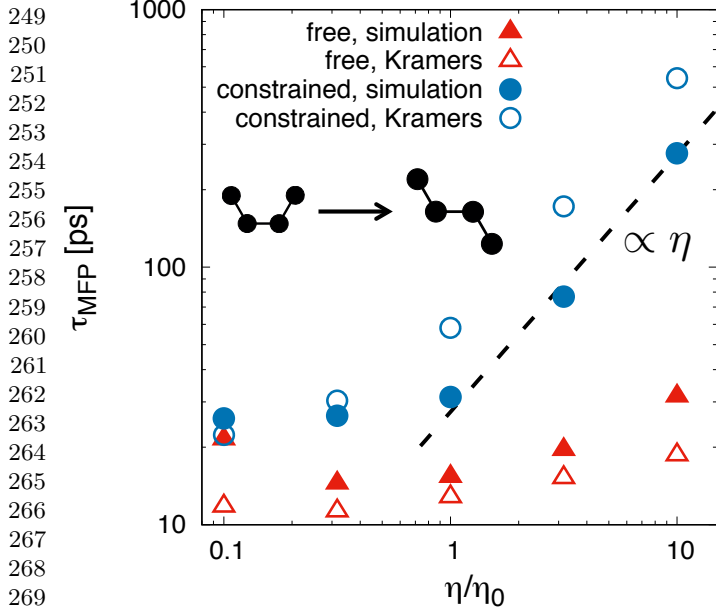
Fig. 2. Mean first passage times τ_{MFP} of the *cis*-to-*trans* transition of the butane dihedral for free (triangles) and constrained (circles) butane extracted from simulation trajectories (filled symbols) are shown as a function of the rescaled water viscosity η/η_0, where η_0 refers to the SPC/E water viscosity. The estimates based on the Kramers formula for medium to strong friction eq. (5) are included as open symbols.

and shows a linear increase of τ_{MFP} with η (indicated by a broken straight line), while for $\eta < \eta_0$ the results for the free and constrained scenarios are rather similar and depend only weakly on η, which will later be explained by inertial effects (i.e. Kramers turnover). The stark deviation between the free and constrained scenarios for $\eta > \eta_0$, amounting to a difference in the reaction times by a factor of ten for the highest viscosity $\eta = 10\eta_0$, is caused by the six additional degrees of freedom for free butane that are orthogonal to the dihedral angle coordinate. Since the dihedral free energy is the same for both scenarios, we conclude that the friction is different in the two scenarios and that this friction difference is caused by the additional degrees of freedom that are present in the free scenario and absent in the constrained scenario. We will later show that the difference in the total friction between the free and constrained scenarios is accompanied by an internal friction contribution for the free case.

B. Memory kernels and friction coefficients. To quantify the friction that acts on the dihedral angle, we map the dynamics of the butane dihedral angle x onto the generalized Langevin equation (GLE)

$$m\ddot{x}(t) = -\int_0^t dt'\,\Gamma(t')\dot{x}(t-t') - \nabla U[x(t)] + F_R(t), \quad [1]$$

where $\Gamma(t)$ denotes the memory kernel. The random force $F_R(t)$ obeys the fluctuation-dissipation theorem and satisfies $\langle F_R(t)F_R(t')\rangle = k_{\mathrm{B}}T\,\Gamma(t-t')$. For vanishing potential, the GLE has been derived by linear projection techniques (4, 5). The mass m is an effective one and follows directly from the simulated dihedral angle trajectory $x(t)$ via the equipartition theorem $m\langle \dot{x}^2\rangle = k_{\mathrm{B}}T$ (see Materials and Methods). The potential $U(x)$ in the GLE is in fact a free energy and follows from the simulated equilibrium probability density along the

reaction coordinate, $p(x)$, as $U(x) = -k_{\mathrm{B}}T\log p(x)$ and is shown in Fig. 1C. To extract $\Gamma(t)$ from simulation trajectories we extend previous methods (38–40) to account for a finite potential $U(x)$. For this we multiply eq. (1) by $\dot{x}(0)$ and average to obtain

$$m\langle \dot{x}(0)\ddot{x}(t)\rangle = -\int_0^t dt'\,\Gamma(t')\left\langle \dot{x}(0)\dot{x}(t-t')\right\rangle - \langle \dot{x}(0)\nabla U[x(t)]\rangle, \quad [2]$$

where we used that the random force is not correlated with the initial velocity, i.e. $\langle \dot{x}(0)F_R(t)\rangle = 0$ (4). Discretizing all functions as $\Gamma_i = \Gamma(i\Delta t)$ with a timestep Δt we obtain the iteration equation

$$\Gamma_i = -\frac{1}{\omega_{i,i}\Delta t C_0^{\dot{x}\dot{x}}}\left(\sum_{j=0}^{i-1}\omega_{i,j}\Delta t\,\Gamma_j C_{i-j}^{\dot{x}\dot{x}} + mC_i^{\dot{x}\ddot{x}} + C_i^{\dot{x}\nabla U}\right), \quad [3]$$

where we defined the correlation function $C_i^{\dot{x}\ddot{x}} = \langle \dot{x}(0)\ddot{x}(i\Delta t)\rangle$ (and similarly $C_i^{\dot{x}\dot{x}}$ and $C_i^{\dot{x}\nabla U}$) and the integration weight $\omega_{i,j} = 1 - \delta_{i,0}/2 - \delta_{i,j}/2$. The correlation function $C_i^{\dot{x}\nabla U} = \langle \dot{x}(0)\nabla U[x(i\Delta t)]\rangle$ is obtained by cubic spline interpolation of $U(x)$. In the SI we demonstrate the numerical robustness of our method.

The extracted memory kernels $\Gamma(t)$ for free butane in Fig. 3B are quite similar for different water viscosities, while for constrained butane the kernels in Fig. 3A differ strongly for different viscosities. In particular, for free butane the long time tail of $\Gamma(t)$, which is mostly responsible for the effective friction, is almost independent of η and oscillations appear that we associate with the presence of orthogonal degrees of freedom. In qualitative accordance with our results in Fig. 2 for the barrier crossing time, we can say that for free butane, the effective friction is less sensitive to solvent viscosity compared to constrained butane.

In Fig. 4, we show the friction coefficient γ for free and constrained butane as a function of water viscosity, which follows from an integral over the memory function according to $\gamma = \int_0^\infty dt\,\Gamma(t)$. For numerical integration, we fit the long time decay of $\Gamma(t)$ by an exponential function (see SI). The friction for constrained butane is linearly proportional to the solvent viscosity, as expected based on the hydrodynamic Stokes equation. To make this more explicit, we denote the translational friction coefficient of a methyl group by $\gamma_{\mathrm{trans}} = 6\pi\eta R_{\mathrm{CH_3}}$. For a methyl group of radius $R_{\mathrm{CH_3}} \approx 0.18\,\mathrm{nm}$ that rotates at a fixed bond angle $\alpha = 111°$ and C–C bond length $l_{\mathrm{B}} = 0.15\,\mathrm{nm}$ around a fixed point in space, which approximates the constrained butane case, we estimate the dihedral friction constant $\gamma = (2\pi/360)^2 (l_{\mathrm{B}}\sin(\alpha))^2 \gamma_{\mathrm{trans}} = 0.01\cdot(\eta/\eta_0)\,\mathrm{u\,nm^2/deg^2\,ps}$, not so different from what we extract from the simulations in Fig. 4 for constrained butane. In contrast, the dynamics of free butane is characterized by a friction coefficient that very weakly depends on the water viscosity, in stark contrast to the hydrodynamic Stokes equation.

C. Internal versus solvent friction. We include empirical fits according to (7, 9, 12)

$$\gamma = (\eta/\eta_0)\,\gamma_{\mathrm{sol,0}} + \gamma_{\mathrm{int}} \quad [4]$$

into Fig. 4 as solid lines. The fits are very good, which validates the assumption of additive solvent and internal contributions. For constrained butane we obtain $\gamma_{\mathrm{int}} =$
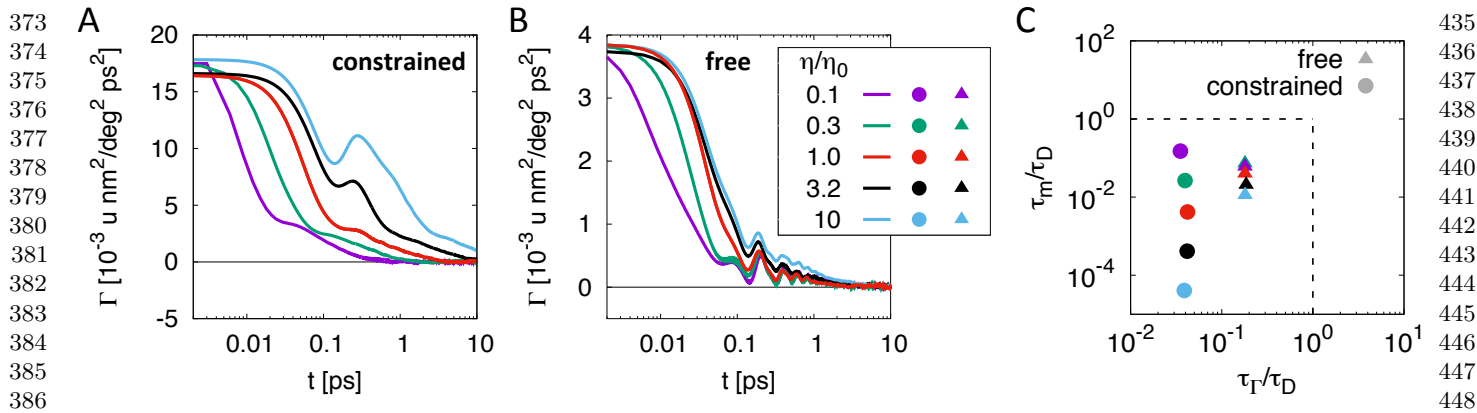
Fig. 3. Memory kernels $\Gamma(t)$ for different rescaled water viscosities η/η_0 extracted from simulation trajectories via eq. (3) for (A) constrained and (B) free butane, where η_0 denotes the SPC/E water viscosity. (C) Inertial and memory timescale ratios τ_m/τ_D and τ_Γ/τ_D calculated from the memory kernels of free and constrained butane for different viscosities, where τ_D denotes the characteristic diffusion time (same color coding as in B).

$1.8 \cdot 10^{-4}\,\mathrm{u\,nm^2/deg^2\,ps}$ and $\gamma_{\mathrm{sol},0} = 3.9 \cdot 10^{-3}\,\mathrm{u\,nm^2/deg^2\,ps}$, which corresponds to a ratio of $\gamma_{\mathrm{int}}/\gamma_{\mathrm{sol},0} = 0.05$ and shows that internal friction is negligible in this case. A small spurious internal friction contribution is in fact expected from the finite difference between the friction coefficient of immobilized and free solutes, as was recently demonstrated based on simulations of methane in water (41). In contrast, for free butane we find $\gamma_{\mathrm{int}} = 5.2 \cdot 10^{-4}\,\mathrm{u\,nm^2/deg^2\,ps}$ and $\gamma_{\mathrm{sol},0} = 6.7 \cdot 10^{-5}\,\mathrm{u\,nm^2/deg^2\,ps}$, and thus a ratio $\gamma_{\mathrm{int}}/\gamma_{\mathrm{sol},0} = 7.7$. Hence, the dynamics of free butane is dominated by internal friction effects for normal water viscosity η_0. The substantial reduction of the solvent friction contribution $\gamma_{\mathrm{sol},0}$ in the free case compared to the constrained case is at first sight surprising. This reduction can be rationalized by the fact that the dihedral angle for free butane is a relative coordinate that depends on the motion of all four carbons and is governed by a relative diffusion constant that results from the weighted sum of the individual carbon diffusion constants.

It remains to be checked whether the friction coefficients we extract from simulation trajectories in Fig. 4 explain the independently measured dihedral barrier crossing times in Fig. 2. This is non-trivial in the present case since, as mentioned earlier, memory and inertia effects invalidate the simple Kramers prediction $\tau_{\mathrm{MFP}} \sim \gamma^{-1}$. To proceed, it is useful to introduce the characteristic time scales of the system. These are the inertial time $\tau_m = m/\gamma$, which measures the time at which ballistic motion crosses over to diffusive motion, the memory time $\tau_\Gamma = \gamma/\Gamma(0)$, which measures the decay time of the memory kernel, and the diffusive time $\tau_D = L^2\gamma/(k_BT)$, which measures the free-diffusion time to advance over a characteristic angle of $L = 60°$. In Fig. 3C we demonstrate that $\tau_m < \tau_D$ and $\tau_\Gamma < \tau_D$ holds for all simulation data, in which case Kramers' formula for the mean first passage time in the medium to strong friction case (6)

$$\tau_{\mathrm{MFP}} = \frac{2\pi\,\omega_{\max}/\omega_{\min}}{[\gamma^2/4 + \omega_{\max}^2]^{1/2} - \gamma/2}\exp\left(\frac{\Delta U}{k_BT}\right), \qquad [5]$$

is expected to be valid. For the barrier height we extract $\Delta U = 3.7\,k_BT$ from the free energy in Fig. 1C, $m\omega_{\max}^2 = 6 \cdot 10^{-3}\,k_BT/\mathrm{deg}^2$ and $m\omega_{\min}^2 = 9 \cdot 10^{-3}\,k_BT/\mathrm{deg}^2$ are the curvatures of the free energy at the maximum and minimum. The results from eq. (5) for free and constrained butane are included as open data points in Fig. 2; the comparison with the

simulation data, which does not use any adjustable parameter, is quite good. The simulation data in the constrained case show a shorter barrier crossing time than expected based on the Kramers formula, whereas for free butane we see the opposite. Both trends can be explained based on memory effects, since an intermediate memory time $\tau_\Gamma/\tau_D \approx 0.01 - 0.1$ significantly accelerates barrier crossing, while a longer memory time increases the barrier crossing time, as has been shown recently (26). Thus, our results for constrained butane presumably correspond to the regime where memory reduces the reaction time, while the results for free butane (which have slightly larger values of τ_Γ/τ_D, as shown in Fig. 3C) correspond to the crossover regime where the memory effect switches from acceleration to slowing down of the reaction time. The saturation of τ_{MFP} for the constrained case in the low-viscosity limit in Fig. 2 is thereby shown to be solely due to inertia effects and thus reflects Kramers turnover, this follows from the fact that the friction γ for the constrained case in Fig. 4 is roughly linear in η over the entire range of water viscosities. In contrast, the behavior of τ_{MFP} for the free case can only be explained by a combination of inertia and internal friction effects. This shows that the present simulation strategy, which compares the free and constrained scenarios and at the same time extracts memory functions, is necessary and useful.

2. Conclusions

The dihedral barrier-crossing dynamics of a constrained butane molecule, where only one carbon atom is allowed to move and thus the dihedral angle is the only degree of freedom (besides solvent degrees of freedom) is shown to be very different from the dynamics of a free butane, where a total of seven positional degrees of freedom are present. This unambiguously demonstrates that friction generated by degrees of freedom that are coupled but orthogonal to the reaction coordinate (in our case the dihedral angle) is dominant in butane. By monitoring the friction, which we directly extract from the memory kernel, as a function of the solvent viscosity, we show that orthogonal degrees of freedom significantly modify the solvent friction contribution and also produce an additional contribution which we denote, in analogy to experiments on protein folding, as internal friction. The internal friction contribution in butane thus stems from the dynamic partitioning of energy over the
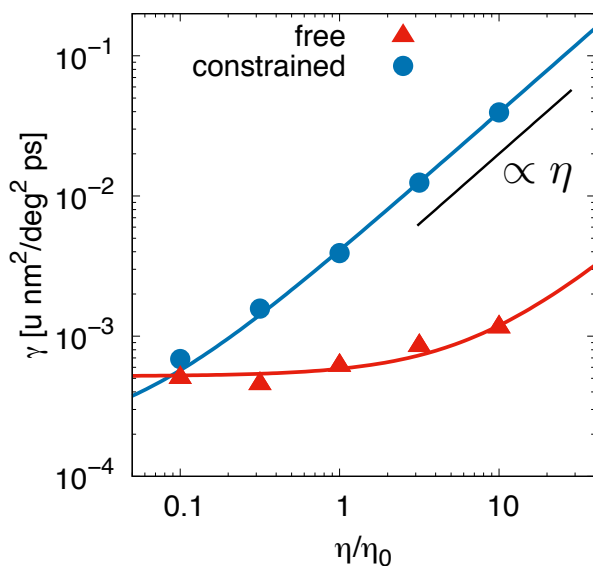
Fig. 4. Friction coefficient γ extracted from the memory kernels in Fig. 3A and B as a function of the rescaled water viscosity η/η_0 for free and constrained butane. Empirical fits according to eq. (4) (denoted by lines) yield internal-to-solvent friction ratios of $\gamma_{\text{int}}/\gamma_{\text{sol},0} = 7.7$ for free and $\gamma_{\text{int}}/\gamma_{\text{sol},0} = 0.05$ for constrained butane.

orthogonal degrees of freedom (which in addition to the six positional also include six conjugate momentum degrees of freedom).

Based on our finding that already for butane, which arguably is a very simple system for which the orthogonal degrees of freedom in fact correspond to the translational and orientational degrees of freedom, internal friction dominates the dynamics, we expect that for larger and more complex molecules, which possess more orthogonal degrees of freedom, internal friction plays an even more important role for the dynamics. For macromolecular conformational transitions where the rate-limiting step involves dihedral angle isomerization (20, 24, 25, 42, 43), our findings constitute one mechanism for the emergence of internal friction effects. But other mechanisms, for example based on interactions between molecular subunits, certainly also exist.

Beyond these applications to polymers and proteins, dihedral isomerization of butane is also interesting in its own right and has been studied by two-dimensional infrared spectroscopy (31). The experimental dihedral isomerization time of a butane derivative solvated in CCl_4 was found to be in the 10 ps range, which agrees with predictions from classical MD simulations (28) and is similar to the simulation results we obtain here. Our analysis thus reveals that in such experiments the internal friction, which for normal water viscosity makes up about 89% of the total friction, dominates the dynamics, a fact that does not transpire from the simulations per se.

It seems difficult to derive the empirical eq. (4), according to which internal and solvent contributions, the latter being defined as the contribution that scales linearly with solvent viscosity η, are additive, from first principles. We note that according to the fluctuation-dissipation theorem the friction coefficient follows from the force-force autocorrelation function (41); a decomposition of the force acting on a reaction coordinate into solute and solvent contributions (which is exactly possible) would necessarily give rise to a solvent, a solute and a mixed solute-solvent contribution, and the linear additivity

in eq. (4) is not obvious. The good comparison between eq. (4) and the simulation data in Fig. 4 validates the linear additivity thus only in a heuristic sense, and could break down for more complicated systems.

Materials and Methods

All simulations are carried out using the GROMACS 5.1 (44, 45) simulation package with double precision. The butane molecule is parameterized by the GROMOS (46) united atom force field, for water we use the SPC/E (47) model. All angles and bonds of water and butane are constrained to their equilibrium values using the SHAKE (48) algorithm. Real butane possesses additional degrees of freedom that we neglect in our classical simulations, namely bond angle and bond length vibrations of carbon-carbon as well as carbon-hydrogen bonds. However, they are not expected to contribute significantly to the dynamics due to the high quantum-mechanical excitation energies for carbon-carbon bonds and due to the relatively small effective mass of carbon-hydrogen bonds. We perform NVT molecular dynamics (MD) simulations and vary the water molecule mass m_{w} in order to change the water viscosity. For water mass larger and equal than the normal water mass, we use a time step of 2 fs, for lighter water mass we lower the timestep by a factor $\eta/\eta_0 \propto \sqrt{m_{\text{w}}}$. The temperature is controlled by the velocity rescaling (49) thermostat at $T = 300\,\text{K}$, which is coupled only to the solvent with a time constant of $\eta/\eta_0 \cdot 1$ ps. In the SI we compare results for the memory kernels calculated from NVT and NVE simulations of a free butane molecule at a water viscosity of $\eta/\eta_0 = \sqrt{10}$ and demonstrate that the ensemble and thus the thermostat have no influence on our results. The equipartition theorem dictates $m\langle \dot{x}^2 \rangle = k_B T$, which is used to extract the effective mass m from the simulated dihedral angle trajectories $x(t)$. For constrained butane, we find values between $m = 0.92 \cdot 10^{-4}\,\text{u nm}^2/\text{deg}^2$ and $m = 1.03 \cdot 10^{-4}\,\text{u nm}^2/\text{deg}^2$, which agree with the expected value for the moment of inertia of a single methyl group of mass $m_{\text{CH}_3} = 15\,\text{u}$ that rotates with a fixed bond angle $\alpha = 111°$ and C–C bond length $l_B = 0.15\,\text{nm}$ around a fixed pivot point, which leads to $m_I = m_{\text{CH}_3}(l_B \sin(\alpha))^2(2\pi/360)^2 = 0.93 \cdot 10^{-5}\,\text{u nm}^2/\text{deg}^2$. For free butane we obtain smaller effective masses between $m = 2.13 \cdot 10^{-5}\,\text{u nm}^2/\text{deg}^2$ and $m = 2.18 \cdot 10^{-5}\,\text{u nm}^2/\text{deg}^2$, as expected for the effective mass that describes a relative coordinate.

1. Bryngelson JD, Wolynes PG (1989) Intermediates and barrier crossing in a random energy model (with applications to protein folding). *J. Phys. Chem.* 93(19):6902–6915.
2. Bryngelson JD, Onuchic JN, Socci ND, Wolynes PG (1995) Funnels, pathways, and the energy landscape of protein folding: A synthesis. *Proteins* 21(3):167–195.
3. Dill KA, Chan HS (1997) From Levinthal to pathways to funnels. *Nat. Struct. Biol.* 4(1):10–19.
4. Mori H (1965) Transport, Collective Motion, and Brownian Motion. *Prog. Theor. Phys.* 33(3):423–455.
5. Zwanzig R (2001) *Nonequilibrium Statistical Mechanics.* (Oxford University Press).
6. Kramers HA (1940) Brownian motion in a field of force and the diffusion model of chemical reactions. *Physica* 7(4):284–304.
7. Ansari A, Jones CM, Henry ER, Hofrichter J, Eaton WA (1992) The role of solvent viscosity in the dynamics of protein conformational changes. *Science* 256(5065):1796–1798.
8. Bieri O, et al. (1999) The speed limit for protein folding measured by triplet–triplet energy transfer. *Proc. Natl. Acad. Sci. U. S. A.* 96(17):9597–9601.
9. Jas GS, Eaton WA, Hofrichter J (2001) Effect of Viscosity on the Kinetics of α-Helix and β-Hairpin Formation. *J. Phys. Chem. B* 105(1):261–272.
10. Pabit SA, Roder H, Hagen SJ (2004) Internal Friction Controls the Speed of Protein Folding from a Compact Configuration. *Biochemistry* 43(39):12532–12538.
11. Qiu L, Hagen SJ (2004) A Limiting Speed for Protein Folding at Low Solvent Viscosity. *J. Am. Chem. Soc.* 126(11):3398–3399.
12. Cellmer T, Henry ER, Hofrichter J, Eaton WA (2008) Measuring internal friction of an ultrafast-folding protein. *Proc. Natl. Acad. Sci. U. S. A.* 105(47):18320–18325.

13. Wensley BG, et al. (2010) Experimental evidence for a frustrated energy landscape in a three-helix-bundle protein family. *Nature* 463(7281):685–688.
14. Soranno A, et al. (2012) Quantifying internal friction in unfolded and intrinsically disordered proteins with single-molecule spectroscopy. *Proc. Natl. Acad. Sci. U. S. A.* 109(44):17800–17806.
15. Borgia A, et al. (2012) Localizing internal friction along the reaction coordinate of protein folding by combining ensemble and single-molecule fluorescence spectroscopy. *Nat Commun* 3:1195.
16. Chung HS, Piana-Agostinetti S, Shaw DE, Eaton WA (2015) Structural origin of slow diffusion in protein folding. *Science* 349(6255):1504–1510.
17. Plaxco KW, Baker D (1998) Limited internal friction in the rate-limiting step of a two-state protein folding reaction. *Proc. Natl. Acad. Sci. U. S. A.* 95(23):13591–13596.
18. Schulz JCF, Schmidt L, Best RB, Dzubiella J, Netz RR (2012) Peptide Chain Dynamics in Light and Heavy Water: Zooming in on Internal Friction. *J. Am. Chem. Soc.* 134(14):6273–6279.
19. Sancho Dd, Sirur A, Best RB (2014) Molecular origins of internal friction effects on protein-folding rates. *Nat. Commun.* 5:5307.
20. Echeverria I, Makarov DE, Papoian GA (2014) Concerted Dihedral Rotations Give Rise to Internal Friction in Unfolded Proteins. *J. Am. Chem. Soc.* 136(24):8708–8713.
21. Zheng W, De Sancho D, Hoppe T, Best RB (2015) Dependence of Internal Friction on Folding Mechanism. *J. Am. Chem. Soc.* 137(9):3283–3290.
22. Zheng W, de Sancho D, Best RB (2016) Modulation of Folding Internal Friction by Local and Global Barrier Heights. *J. Phys. Chem. Lett.* 7(6):1028–1034.
23. Klimov DK, Thirumalai D (1997) Viscosity Dependence of the Folding Rates of Proteins. *Phys. Rev. Lett.* 79(2):317–320.
24. Portman JJ, Takada S, Wolynes PG (2001) Microscopic theory of protein folding rates. II. Local reaction coordinates and chain dynamics. *J. Chem. Phys.* 114(11):5082–5096.
25. Best RB, Hummer G (2006) Diffusive Model of Protein Folding Dynamics with Kramers Turnover in Rate. *Phys. Rev. Lett.* 96(22):228104.
26. Kappler J, Daldrop JO, Brünig FN, Boehle MD, Netz RR (2017) Memory-induced acceleration and slowdown of barrier crossing. *J. Chem. Phys.* accepted.
27. Chandler D (1978) Statistical mechanics of isomerization dynamics in liquids and the transition state approximation. *J. Chem. Phys.* 68(6):2959–2970.
28. Rosenberg RO, Berne BJ, Chandler D (1980) Isomerization dynamics in liquids by molecular dynamics. *Chem. Phys. Lett.* 75(1):162–168.
29. Knauss DC, Evans GT (1980) Liquid state torsional dynamics of butane: The Kramers rate and the torsion angle correlation times. *J. Chem. Phys.* 73(7):3423–3429.
30. Evans GT (1980) Momentum space diffusion equations for chain molecules. *J. Chem. Phys.* 72(7):3849–3858.
31. Zheng J, Kwak K, Xie J, Fayer MD (2006) Ultrafast Carbon-Carbon Single-Bond Rotational Isomerization in Room-Temperature Solution. *Science* 313(5795):1951–1955.
32. Kuhn W, Kuhn H (1946) Modellmässige Deutung der inneren Viskosität (der Formzähigkeitskonstante) von Fadenmolekeln I. *Helv. Chim. Acta* 29(3):609–626.
33. Khatri BS, McLeish TCB (2007) Rouse Model with Internal Friction: A Coarse Grained Framework for Single Biopolymer Dynamics. *Macromolecules* 40(18):6770–6777.
34. Soranno A, et al. (2017) Integrated view of internal friction in unfolded proteins from single-molecule FRET, contact quenching, theory, and simulations. *Proc. Natl. Acad. Sci. U. S. A.* 114(10):E1833–E1839.
35. Avdoshenko SM, Das A, Satija R, Papoian GA, Makarov DE (2017) Theoretical and computational validation of the Kuhn barrier friction mechanism in unfolded proteins. *Sci. Rep.* 7.
36. Pastor RW, Karplus M (1989) Inertial effects in butane stochastic dynamics. *J. Chem. Phys.* 91(1):211–218.
37. Zuckerman DM, Woolf TB (2002) Transition events in butane simulations: Similarities across models. *J. Chem. Phys.* 116(6):2586–2591.
38. Berne BJ, Harp GD (1970) On the Calculation of Time Correlation Functions in *Advances in Chemical Physics*, eds. Prigogine I, Rice SA. (John Wiley & Sons, Inc.), pp. 63–227.
39. Lange OF, Grubmüller H (2006) Collective Langevin dynamics of conformational motions in proteins. *J. Chem. Phys.* 124(21):214903.
40. Shin HK, Kim C, Talkner P, Lee EK (2010) Brownian motion from molecular dynamics. *Chem. Phys.* 375(2–3):316–326.
41. Daldrop JO, Kowalik BG, Netz RR (2017) External Potential Modifies Friction of Molecular Solutes in Water. *Phys. Rev. X* 7(4):041065.
42. Kuhn W, Kuhn H (1945) Bedeutung beschränkt freier Drehbarkeit für die Viskosität und Strömungsdoppelbrechung von Fadenmolekellösungen I. *Helv. Chim. Acta* 28(1):1533–1579.
43. Guo Z, Thirumalai D (1995) Kinetics of protein folding: Nucleation mechanism, time scales, and pathways. *Biopolymers* 36(1):83–102.
44. Hess B, Kutzner C, van der Spoel D, Lindahl E (2008) GROMACS 4: Algorithms for Highly Efficient, Load-Balanced, and Scalable Molecular Simulation. *J. Chem. Theory Comput.* 4(3):435–447.
45. Abraham MJ, et al. (2015) GROMACS: High performance molecular simulations through multi-level parallelism from laptops to supercomputers. *SoftwareX* 1–2:19–25.
46. Oostenbrink C, Villa A, Mark AE, Van Gunsteren WF (2004) A biomolecular force field based on the free enthalpy of hydration and solvation: The GROMOS force-field parameter sets 53a5 and 53a6. *J. Comput. Chem.* 25(13):1656–1676.
47. Berendsen HJC, Grigera JR, Straatsma TP (1987) The missing term in effective pair potentials. *J. Phys. Chem.* 91(24):6269–6271.
48. Ryckaert JP, Ciccotti G, Berendsen HJC (1977) Numerical integration of the cartesian equations of motion of a system with constraints: molecular dynamics of n-alkanes. *J. Comput. Phys.* 23(3):327–341.
49. Bussi G, Donadio D, Parrinello M (2007) Canonical sampling through velocity rescaling. *J. Chem. Phys.* 126(1):014101.